RSC Advances

ROYAL SOCIETY OF CHEMISTRY

www.rsc.org/advances

RSC Advances

ARTICLE

Low temperature synthesis and characterization of the substitutional Na-modified $K_2Ti_6O_{13}$ nanobelts with improved photocatalytic activity under UV irradiation

Qiang Wang, Qingjun Guo and Bing Li*

Received 00th January 20xx,
Accepted 00th January 20xx

DOI: 10.1039/x0xx00000x

www.rsc.org/

The substitutional Na-modified $K_2Ti_6O_{13}$ (NKTO) nanobelts were synthesized by a facile one-step method from NaCl-KCl melts at a relatively low temperature below 700℃. The obtained samples were fully characterized by X-ray diffraction (XRD), energy dispersive spectrometer (EDS), scanning electron microscopy (SEM), transmission electron microscopy (TEM), high-resolution transmission electron microscopy (HRTEM), selected area electron diffraction (SAED), thermogravimetry and diferential scanning calorimetry (TG-DSC), N_2 adsorption-desorption analysis, UV-vis diffuse reflectance spectroscopy and photoluminescence (PL) spectrum. The results revealed the highly crystalline NKTO nanobelts obtained above 680℃ exhibited not only a narrow distribution of particle size but well dispersivity. The replacement of K^+ by Na^+ ions reduced the interplanar spacing of $K_2Ti_6O_{13}$ but did not destroy its oriented growth along [010]. From these results, the formation mechanism of the NKTO nanobelts was proposed. The spectific surface area of the nanobelts showed a decrease with the increasing of synthetic temperature. Different titania phases were found to have a significant effect on the formation of NKTO nanobelts and rutile was the optimum titanium precursor. Substitutional Na-modifying was demonstrated to not only red-shift the absorption edge and increase UV absorption but efficiently suppress the recombination of photogenerated electron-hole pairs. The photocatalytic tests showed the substitutional Na modifying and lower synthetic temperature greatly promoted the activity for photodegration of methyl orange under UV irradiation and the improved photocatalytic mechanism was also discussed.

1. Introduction

Alkal metal hexatitanates, $M_2Ti_6O_{13}$ (M=Li, Na, K, Rb, Cs), with unique tunnel or layer crystalline structures have attracted increasing interest due to their excellent thermal durability, chemical resistivity, mechanical performance, ion-exchange properties and photocatalytic activity.[1-11] Especially, $K_2Ti_6O_{13}$ and $Na_2Ti_6O_{13}$ have been studied to be adequate for the degradation of toxic substances,[10-14] decomposition of pure water[15-17] as well as for oxygen electrodes in potentiometric sensors[18] owing to their better photocatalytic properties under UV irradiation. They are traditionally prepared by calcination method,[19-21] hydrothermal synthesis,[22-25] sol-gel technique[14,26] and molten salt synthesis (MSS)[27-30]. Among these synthesis methods, MSS has been proved to be one of the simplest, most versatile, and cost-effective approaches available for obtaining crystalline, chemically purified, single-phase and non-agglomerated powders at lower calcination temperature than the conventional soild-state reaction and always in overall shorter reaction time as compared with hydrothermal synthesis.[31,32]

However, a heating temperature above 900□ is usually needed to obtain highly crystalline one-dimensional alkali-metal hexatitanates (such as $K_2Ti_6O_{13}$ and $Na_2Ti_6O_{13}$) crystals from molten chloride salts. Sometimes, in order to favor synthesizing reaction and improve uniformity of the fibrous products, a nonionic surfactant like NP-9 (nonylphenol polyethylene glycol ether) will be introduced into the molten salts,[28,33,34] which increases the production cost. Therefore, developing a facile and low-temperature (<900□) MSS of well-crystalized fibrous hexatitanates is still worth considering further. Moreover, the obtained single-phase $K_2Ti_6O_{13}$ products can't perform as well as expected in photocatalytic reactions due to its wide band gap, high recombination rate of photogenerated electron-hole pairs and small specific surface area. As a result, a great effort has been devoted to improve the photocatalytic activity of $K_2Ti_6O_{13}$. For example, Tretyachenko et al. reported nanostructured potassium titanates modified using transition metals exhibit a

School of Mechanical and Power Engineering, East China University of Science and Technology, 130Meilong Road, Shanghai 200237,China. E-mail: drlibing@163.com; Tel: +86-21-64252601

higher photocatalytic activities in the ultraviolet and visible ranges.[35] Amano et al. prepared Pt-loaded nanowire-structured potassium titanate to improve photocatalytic activity.[36] Several researchers investigated the photocatalytic properties of titanates containing different amounts of alkaline ions.[9,37] Park also reported that the hydroxyapatite precipitation could enhance the photocatalytic activity of $K_2Ti_6O_{13}$ whiskers.[10] These modification methods above often include two steps, i.e., preparation of pure titanates and the following modified treatments.

Untile now, however, no reports on one-step synthesis of Na-modified $K_2Ti_6O_{13}$ (referred hereafter as NKTO) nanostructures with improved photocatalytic activity via MSS method below 700□ have been published. The NaCl-KCl eutectic salts with lower melting point than KCl (657 □ vs. 771 □) can be used as solvent, which contributes to the growth of smaller particle size, i.e. larger surface area. Such a large surface area is favorable to the enchanced photocatalytic properties, because it can promote adsorption, desorption and diffusion of reactants and products. It was reported that the activity of hexatitanates photocatalytic water-splitting was associated with their efficiency to produce photoexcited charge carriers and at the same time limitted by the recombination rate of photoexcited electron-hole pairs.[17] However, during the growth of $K_2Ti_6O_{13}$ crystals in the NaCl-KCl molten salts, K^+ ions in the tunnel structures can be partially replaced by smaller Na^+ ions from the melts to product NKTO nanobelts,[38] which may change pristine crystal and band structures and so provides a great potential driving force to suppress the recombination of photogenerated electron-hole pairs, thus resulting in the enhancement of photocatalytic activity.

Here, we reported for the first time, that the NKTO nanobelts were synthesized by one-step MSS method below 700□ increasing the specific surface area of the products and successfully incorporating Na^+ into $K_2Ti_6O_{13}$. The crystal stucture, chemical composition, morphology and optical properties of the NKTO nanobelts were systematically characterized by XRD, EDS, SEM, TEM, SAED, HRTEM, TG-DSC, N_2 adsorption-desorption analysis and UV-vis diffuse reflectance spectroscopy combined with PL spectra. Based on the results, the formation mechanism of NKTO nanobelts was proposed. The effect of different titania phases on the formation of NKTO nanobelts was also investigated. The improved photocatalytic activity of the synthesized samples was evaluated by photodegradation of MO solution under UV irradiation and correspondingly the photocatalytic mechanism was also discussed.

2. Experimental

2.1 Materials

The starting materials used in this study included rutile and anatase TiO_2 nanoparticles (50 nm), K_2CO_3, Na_2CO_3 (AR, Xiya Reagent, Ltd), KCl and NaCl (AR, Sinopharm Chemical Reagent Co., Ltd). All the materials were used without any further purifications.

2.2 Sample preparation

In a typical procedure, K_2CO_3 and rutile TiO_2 were mixed with NaCl-KCl eutectic salts (50 mol% NaCl + 50 mol% KCl) at a molar ratio of 1:5.5:110, and ground homogenously in an agate mortar under ethyl alcohol for 30 min. The obtained mixture were dried and transferred into a corundum crucible. After that, the crucible was heated to 660 □ (680 □,700 □) with a heating rate of 5 □/min and held for 3 h at the required temperature and then cooled naturally to room temperature. The resulted products were washed with deionized water repeatedly to remove the residual NaCl-KCl and finally dried overnight in air at 100 □. The obtained products were named as NKTO-660, NKTO-680 and NKTO-700, respectively.

In order to study the effect of different titania phases on the formation of products, anatase TiO_2 was selected as titanium precursor to synthesize the samples at 660 □ (not given), 680 □ (not given), 700 □, 800 □ (NKTO-800), 900□ (NKTO-900) for 3 h by the same procedure mentioned above. The samples synthesized at 900□ from KCl melt (KTO-900) and from NaCl melt (NTO-900) were also obtained as the referential materials.

2.3 Characterizations

The crystalline phase and crystal lattice parameters of the as-synthesized samples were determined by XRD (D/max 2550V) with Cu-K*a* radiation (λ=1.54 Å). Morphology, chemical compositions and microstructure of the samples were characterized by SEM (JEOL JSM-6360LV), TEM (JEM-2100, 200 kv) equipped with EDS (VARIO EL□). HRTEM images and SAED patterns were also obtained on the JEM-2100 microscope operated at an acceleration voltage of 200 kV to investigate the crystallinity and growth direction of samples. TG-DSC analysis was measured by an STA 449F3 thermal analyzer (Netzsch, Germany) to study the formation mechanism of NKTO nanobelts. The optical properties of the samples are studied by UV-vis diffuse reflectance spectra using an Ultraviolet-obviously-near-infrared spectrophotometer (UV-VIS-NIR, American Varian Cary 500) and PL spectrum measured at room temperature with a fluorescence spectrofluorometer (Jobin Yvon Inc. Fluorolog-3). The specific surface area of the samples were deduced by the BET method using a Macromeritics ASAP2460 apparatus.

2.4 Photocatalytic activity tests

The photocatalytic activity of the as-synthesized samples was evaluated by photodegradation of MO solution (300 ml, 10 ppm) placed in a glass in the presence of 0.3 g as-synthesized samples under irradiation of a TUV8W/G8/T5 UV lamp at room temperature. Prior to UV irradiation, the suspension is

magnetically stirred in dark for 1 h to reach absorption-desorption equilibrium. At certain time intervals, a 10 ml aqueous suspension was taken with syringe filter unit (Millipore, pore size 0.22 μm) and centrifuged to remove the photocatalyst particles which could be recycled. The variations of characteristic absorbance intensity in the UV-vis absorption spectra of MO at λ=465 nm was monitored on a ultraviolet-visible-near infrared spectrophotometer (American Varian Cary 500) to evaluate the photocatalytic degradation efficiency (η). Herein, η was calculated by the following formula:

$$\eta = \left(\frac{C_0 - C_t}{C_0}\right) \times 100\% = \left(\frac{A_0 - A_t}{A_0}\right) \times 100\% \qquad (1)$$

where C_0 is the concentration of MO solution at absorption-desorption equilibrium, C_t is the time dependent concentration; A_0 and A_t are the corresponding absorbance values, respectively.

3. Results and discussion

3.1 Structural and morphological characterizations

Fig. 1 (combined with Fig. S1) shows the XRD patterns of the samples synthesized from NaCl-KCl molten salts at different synthetic temperature, which clearly reveals they can be indexed to $K_2Ti_6O_{13}$ phase (monoclinic structure, space group C2/m(12), JCPDS Card No.74-0275), without any noticeable peaks belonging to the unreacted TiO_2 or $Na_2Ti_6O_{13}$ (Fig. S2), indicating the starting materials (TiO_2, K_2CO_3) have been almost transformed into $K_2Ti_6O_{13}$ products even at 660 □ and TiO_2 does not react with NaCl melt yielding $Na_2Ti_6O_{13}$ phase under current synthetic conditions. The sharp and intense peaks indicate that the samples are highly crystalline. It is worth noting that the diffraction peaks of these samples present a slight shift to higher 2θ position compared to the standard XRD pattern of $K_2Ti_6O_{13}$, which can be attributed to the fact that the potassium ions in tunnel crystalline structure of $K_2Ti_6O_{13}$ have been locally replaced by smaller sodium ions from NaCl-KCl melts, in other words, the decrease of interplanar spacing results from the ion replacement of K^+ by Na^+. This is also confirmed by the EDS analysis. As shown in Fig. 2, the representative EDS spectra of NKTO-680 reveals that a certain amount of sodium element is detected. In Table 1, the chemical composition of the as-synthesized samples show the molar ratio of (Na+K)/Ti for these samples are all close to 1:3, defining the chemical formula of $Na_{0.88}K_{1.12}Ti_6O_{13}$ averagely, i.e., the Na^+ ions incorporated into the crystal lattice of $K_2Ti_6O_{13}$ are not interstitial but substitutional, which is consistent with the result of XRD analysis. We can conclud that, therefore, highly crystalline substitutional Na-modified $K_2Ti_6O_{13}$ crystals have been synthesized directly below 700 □ from NaCl-KCl melts.

The morphology and dimensions of as-synthesized NKTO products were characterized by SEM. It can be seen in Fig. 3a combined with Fig. 3b that the sample NKTO-660 mainly consists of nonuniform and agglomerated belt-like products mixed with some particles, which suggests the heating temperature is so low that NaCl-KCl melts can not provide an enough homogeneous liquid phase for crystal growth. As the temperature increasing to 680 □, a large quantity of well-formed nanobelts with a typical thickness of 100-200 nm and a length in excess of 5 um are observed in Fig. 3c. The fibrous morphology of NKTO can be attributed to its unique rectangular tunnel crystal structure. Similar to Fig. 3c, Fig. 3d shows that the non-agglomerated NKTO nan-

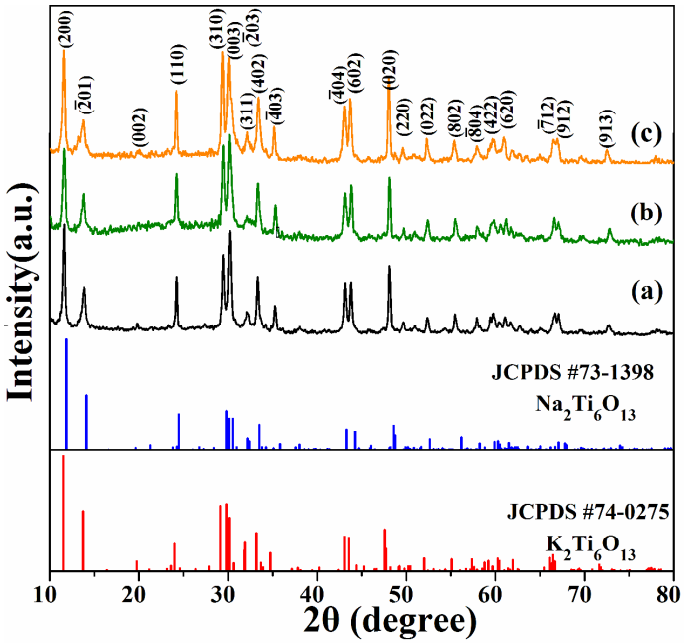

Fig. 1 XRD patterns of the as-synthesized samples: (a) NKTO-660, (b) NKTO-680 and (c) NKTO-700 and the bar chart shows the standard XRD pattern of $K_2Ti_6O_{13}$ (JCPDS Card No.74-0275) and $Na_2Ti_6O_{13}$ (JCPDS Card No.73-1398).

Table 1 Chemical composition of the as-synthesized NKTO nanobelts samples.

samples	Na (at %)	K (at %)	Ti (at %)	O (at %)	Al(at %)	C (at %)	(Na+K)/Ti
NKTO-660	4.54	5.48	30.79	54.78	0.28	4.13	0.33
NKTO-680	4.96	5.64	32.04	53.28	0.29	3.79	0.32
NKTO-700	4.38	6.08	31.07	54.31	0.31	3.85	0.33

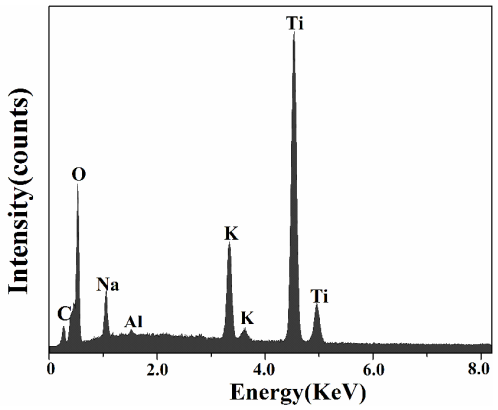

Fig. 2 EDS spectra of the sample NKTO-680. The presence of Al peak likely originates from the contamination of alumina crucibles during the synthesis.

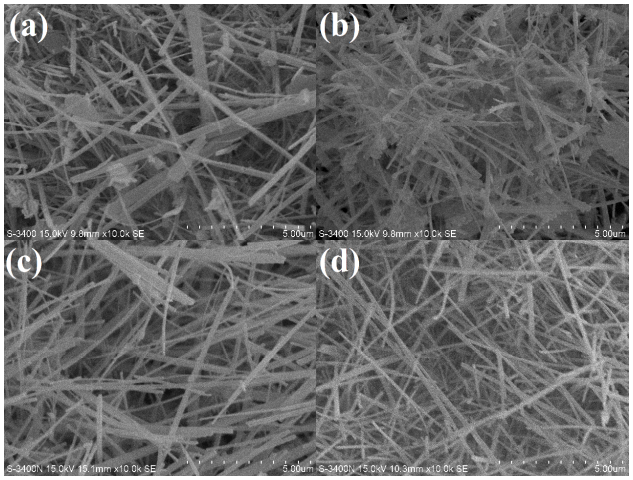

Fig. 3 SEM images of the as-synthesized samples: (a-b)NKTO-660, (c) NKTO-680, (d) NKTO-700.

obelts are obtained at 700 □ and the size distribution is relatively narrow.

The crystal structure of the obtained nanobelts were further characterized with TEM. Fig. 4a is a typical TEM image of the sample NKTO-680 showing the products consist of uniform nanobelts with a flat and smooth surface. Fig. 4b shows a high magnification TEM image of an individual nanobelt with the width of about 110 nm and the SAED pattern (Fig. 4c) taken on it indicates the NKTO nanobelt has a preferential growth along [010] crystallographic direction, which is in good agreement with $K_2Ti_6O_{13}$ and also further suggests the substitutional Na modifying do not destroy the oriented growth of $K_2Ti_6O_{13}$ nanobelts.[5,29] The streaking between the diffraction spots shown in SEAD pattern may be attributed to a small amount of crystal defect in the nanobelts result from the replacement of K^+ ions by smaller Na^+ ions. The corresponding HRTEM image in Fig. 4d shows that the lattice fringe of this nanobelt is examined to be 0.186 nm, which is smaller than the standard interplanar spacing value (0.191 nm) of (020) planes of $K_2Ti_6O_{13}$, consistent with the result of XRD. Therefore, the crystal structure of the as-synthesized NKTO nanobelts can be illustrated as Fig. 5.

3.2 The formation mechanism of NKTO nanobelts

Based on the above characterization results and previous related studies,[39] a possible formation mechanism of NKTO nanobelts was proposed as illustrated in Fig.6. Firstly, the starting materials (rutile TiO_2, K_2CO_3, KCl-NaCl) are mixed evenly so that the reactants including nanosized TiO_2 and K_2CO_3 particles are well dispersed in the NaCl-KCl salts used as reaction medium (Fig. 6a). Next, in Fig. 6b, when the calc-

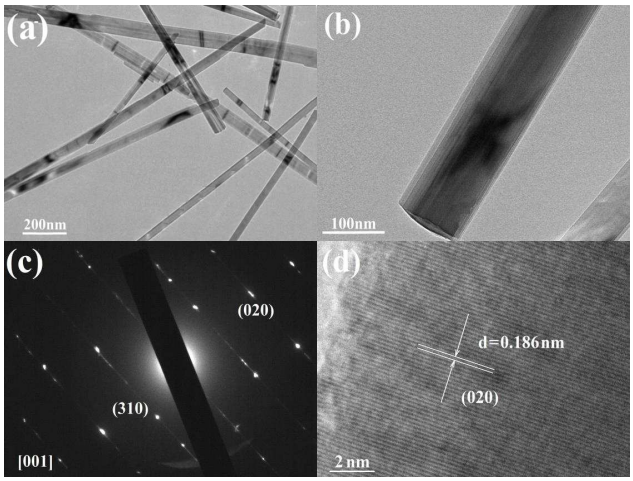

Fig. 4 (a) A typical TEM image of the sample NKTO-680. (b) A high magnification TEM image of an individual NKTO-680 nanobelt. (c)The selected area electron diffraction (SAED) pattern of the individual nanobelt (shown in Fig.4b) recorded along the [001] zone axis. (d)The HRTEM image corresponding to SEAD pattern.

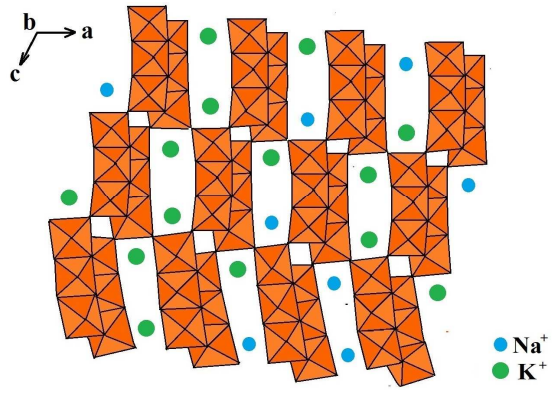

Fig. 5 Crystal structure of the as-synthesized NKTO nanobelts along the [010] direction.[24] K^+ and the substitutional Na^+ ions are located into the rectangular tunnel structures consisting of adjacent [TiO_6] octahedra.

ination temperature rises higher than the eutectic point of NaCl-KCl (657 □), NaCl-KCl salts become into the homogeneous liquid melts and simultaneously K_2CO_3 begin to be dissolved in it, while TiO_2 can agglomerate with each other and grow to form bigger rod-like bulks as TiO_2 has no solubility in molten chlorides.[34] Then as shown in Fig. 6c, the molten K_2CO_3 diffusing randomly in the melts as K^+ and CO_3^{2-} ions forms will react with TiO_2 bulks at the solid-liquid interface to yeild $K_2Ti_6O_{13}$ nuclei (as the templates for further grow) and CO_2 gas, which can be described by the following formula :

$$K_2CO_3 + 6\,TiO_2 \rightarrow K_2Ti_6O_{13} + CO_2\uparrow \qquad (2)$$

According to the dissolution-precipitation mechanism,[40] with the continuous precipitation and consumption of K_2CO_3 on the templates, the reaction (2) proceeds continually and naturally the $K_2Ti_6O_{13}$ nuclei grow further along the preferential crystallization direction gradually to form one-dimensional nanocrystals. During this process, the K^+ ions in $K_2Ti_6O_{13}$ nanostructures will be replcaed by the smaller Na^+ ions from the NaCl-KCl melts. In such way, a large quantity of well-crystallized and uniform NKTO nanobelts are obtained finally (Fig. 6d). It should be mentioned that the large amout of NaCl-KCl melts provided a desired environment for the growth of NKTO nanocrystals and at the same time prevented the agglomeration of the formed NKTO nanobelts.

Then as shown in Fig.7, the TG-DSC curves for NKTO precursor was used to support the formation mechanism proposed above. The TG results suggest the sample loses weight about 1.8% slowly from 60 to 90 □ corresponding to the endothermic peak at 84.7 □ in the DSC curve, which may be due to volatilization of physically absorbed water. As the temperature increases from 650 to 1000 □, the sample exhibits further and sharper weight loss about 67.1%, which is mainly due to the reaction (2) releasing CO_2 and the evaporation of NaCl-KCl molten salts supported by the endothermic peak at 929.2 □ in the DSC curve.[41] Note that the sharp endothermic peak of DSC at 664.5 □ corresponds to not only the melting of NaCl-KCl salts (657 □) and the occurring of reaction (2) but also the ions exchange of K^+ in the tunnel crystal structure of $K_2Ti_6O_{13}$ by Na^+ ions from the molten salts.

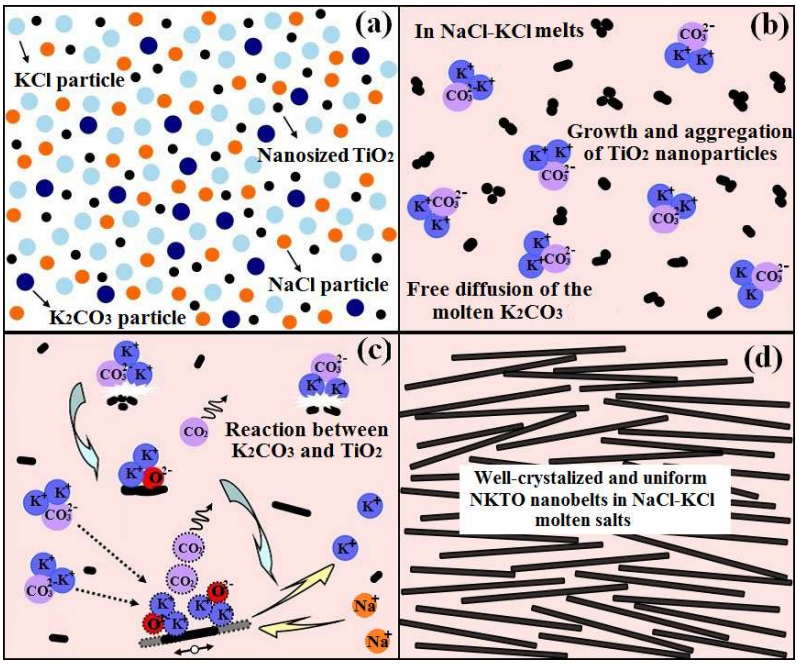

Fig.6 (a-d) Schematic illustrations of the formation mechanism of NKTO nanobelts in NaCl-KCl melts.

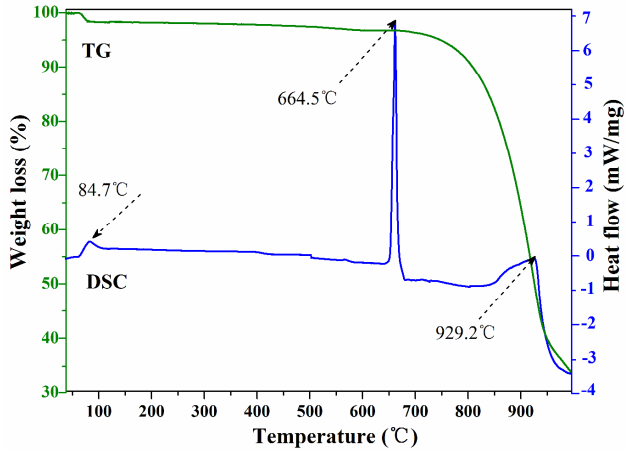

Fig.7 (a-d) TG-DSC curves for the NKTO precursor.

3.3 N_2 adsorption-desorption isotherm analysis

In order to characterize the specific surface areas and the porosity of the as-synthesized NKTO nanobelts, the nitrogen adsorption-desorption measurements were carried out and the results were shown in Fig. 8. According to the Brunauer-Deming-Deming-Teller (BDDT) classification,[42] the isotherm of NKTO-660 can be nearly categorized as type IV with small H_3 type hysteresis loop observed in the range (P/P_0) of 0.5~1.0, suggesting the presence of mesoporous structures. The hysteresis loop in the low pressure range ($0.5< P/P_0 <0.9$) is associated with the intra-aggregated pores made by the agglomerate of nanobelts and particles observed in SEM images. The high-pressure hysteresis loop ($0.9< P/P_0 <1$) is related to the larger pores formed between secondary particles.[43] While the isotherms of both NKTO-680 and NKTO-700 can be attributed to type II, which indicates the presence of macroporous structures, i.e., the nanobelts are well dispersive. The BET specific surface area (S_{BET}) of samples (NKTO-660/680/700) are calculated to be 16.53 m^2/g, 13.87 m^2/g and 13.02 m^2/g respectively, highlighting the decrease of surface area with the increasing of synthetic temperature. This decreased S_{BET} is due to the fact that the higher synthetic temperature promotes the crystal growth of NKTO leading to the formation of bigger particles, and compared with 1-dimensional nanobelts, 0-dimensional nanoparticles (in NKTO-660) have higher surface-to-volume ratio, which means larger surface area.

3.4 Effects of different titania phases on the formation of NKTO from NaCl-KCl melts

Aiming to identify the effect of different titania phases on the formation of NKTO, the XRD patterns of the samples synthesized using anatase as Ti precursor are shown in Fig. 9 (and Fig. S3). The results reveal that the products obtained at 700 □ consist of two kinds of crystalline phases, i.e., anatase TiO_2 and NKTO, specially, the diffraction intensity from anatase phase is higher compared with that of NKTO phase, indicating the amount of unreacted anatase is relatively large. With the increasing of synthetic temperature, the anatase phase can change into NKTO completely until 800 □ and the resulted single-phase NKTO is stable at 900 □. These observations clearly suggests that anatase TiO_2 isn't favorable to low temperature (<700 □) synthesis of NKTO nanbelts from NaCl-KCl melts, in other words, rutile is the optimum titanium precursor.

Besides, it can be seen that the synthesis preformed in KCl melt at 900 □ have yielded a pure $K_2Ti_6O_{13}$ (JCPDS Card No.74-0275) phase and single-pahse $Na_2Ti_6O_{13}$ (JCPDS Card No.73-1398) has been also obtained from NaCl melt at 900 □. It is worth noting that the diffraction peaks for NKTO-900 become sharper compared with KTO-900, suggesting an effective enhancement of crytallization and grain growth in NaCl-KCl molten salts.[41]

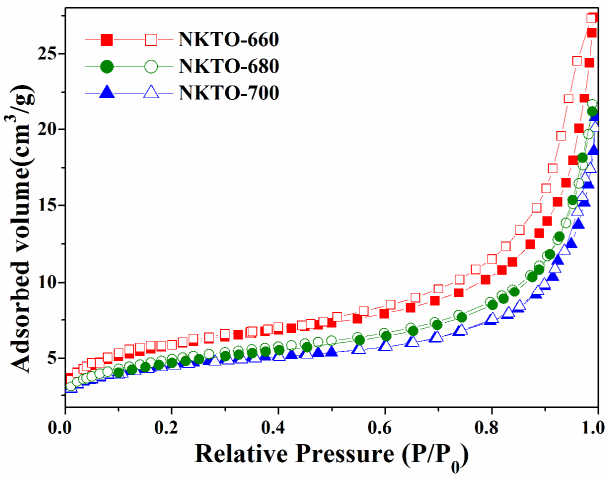

Fig. 8 The nitrogen adsorption-desorption isotherms of the as-synthesized samples.

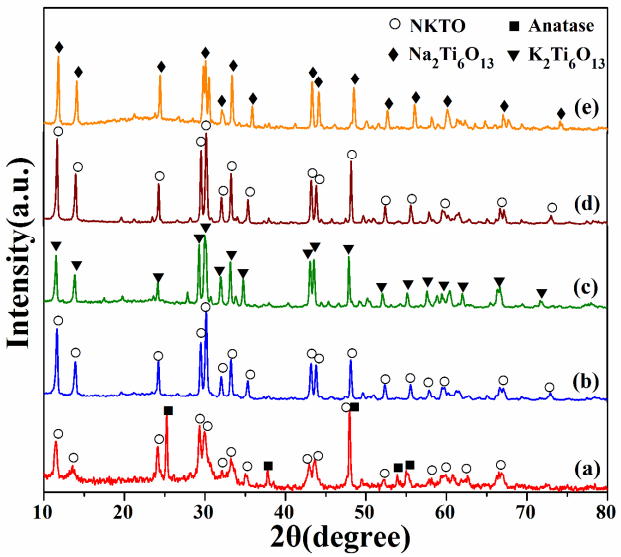

Fig. 9 XRD patterns of the samples synthesized using anatase as Ti precursor at different synthetic temperature: (a)700, (b) NKTO-800, (c) KTO-900, (d) NKTO-900, (e) NTO-900.

3.5 Optical properties

As shown in Fig.10a, the optical properties were investigated firstly through UV-Vis diffuse reflection spectra. From these spectra, the band gap energy (E_g) of the as-synthesized samples can be calculated using the equation:

$$\alpha h\nu = A(h\nu - E_g)^{1/2} \qquad (3)$$

where α is the absorption coefficient, hν is the photon energy and A is a constant.[44] The simplification of the above equation into the formula:

$$E_g = \frac{1240.82}{\lambda} \qquad (4)$$

where λ is the absorption band edge wavelength.[45]

The absorption intensity in ultraviolet region exhibited an enhancement with the increasing of synthetic temperature, as observed in Fig. 10a, indicating that NKTO-700 can absorb more light and induce more photogenerated electrons and holes available for photocatalytic reaction than both NKTO-660 and NKTO-680,[46] and the absorption edge of these samples are all located at around 370 nm that corresponds to the E_g of ~ 3.35 eV. As shown in Fig. 10b, the Eg of KTO-900 and NTO-900 can be caluated to be about 3.42 eV and 3.48 eV, respectively, which is consistent with the previous reports.[34,47] Combined with the inset, a red shift is found for NKTO-900 compared with KTO-900 and NTO-900, and the absorption intensity of the spectrum for NKTO-900 is enhanced obviously in ultraviolet region. NKTO-900 also has the same Eg with NKTO-800 of ~ 3.35 eV, while the latter obviously has stronger optical absorption than the former.

In order to investigate the effect of Na modifying on the transfer and lifetime of photogenerated charge carriers in photocatalyst particles, the room temperature PL spectra for NTO-900, KTO-900 and NKTO-900 under an excitation wavelength of 325 nm were carried out. The results presented in Fig.11 show that they can exhibit strong and broad emission in the wavelength range of about 400-700 nm, whereas the peak intensities of NKTO-900 are signicantly lower than that of KTO-900 and NTO-900. Considering the PL emission originates from the recombination of photogenerated electron-hole pairs, the decreased peak intensity suggest that NKTO-900 exhibits lower electrons-holes recombination rate compared with both of KTO-900 and NTO-900. When the recombination rate decreases, more photogenerated charge carriers can participate in the photochemical transformation, resulting in the enhanced photocatalytic activity.

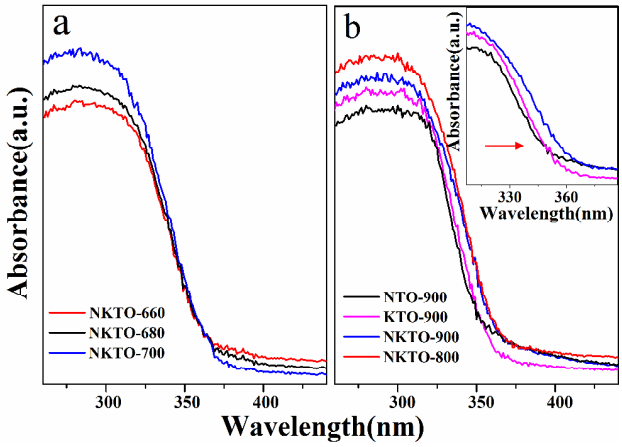

Fig.10 (a) UV-Vis diffuse reflection spectra of the as-synthesized NKTO nanobelts; (b) UV-Vis diffuse reflection spectra for KTO-900, NTO-900, NKTO-900, NKTO-800. The inset shows the enlarged UV-Vis spectra.

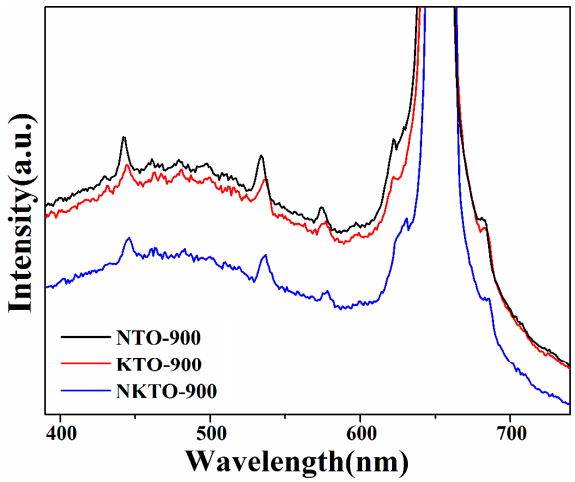

Fig. 11 The room temperature PL spectra for NTO-900, KTO-900 and NKTO-900.

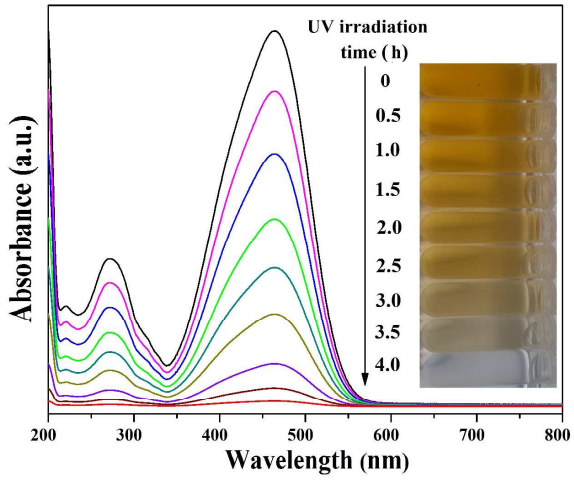

Fig. 12 (a) Temporal evolution of the UV-Vis spectra and color (inset) of MO solution in the presence of 0.3 g as-synthesized NKTO-660 nanobelts under UV irradiation.

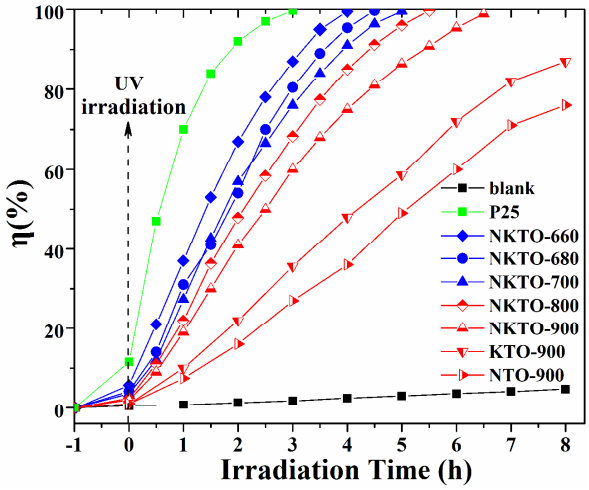

Fig. 12 (b) Photocatalytic degradation of methyl orange by the as-synthesized samples under UV irradiation. The blank experiment is also shown in the figure.

3.6 Photocatalytic evaluation

The photocatalytic activity of the NKTO samples was evaluated by photodegradation of MO in the catalyst suspension under UV light, in comparison with those of the pure $K_2Ti_6O_{13}$, $Na_2Ti_6O_{13}$ samples and Degussa P25 powders. In the tests, with the increasing of UV irradiation time, the suspension in the present of as-synthesized photocatalysts faded rapidly from orange to approximately colorless, while the blank experiment indicates the photodegradation of MO is negligible. Fig. 12a presents clearly the temporal evolution of UV-Vis spectra and color (inset) of MO solution mediated by NKTO-660 nanobelts. It can be observed from Fig. 12b that the photocatalytic activity of the samples obtained below 700 □ increase in the order of NKTO-660 > NKTO-680 > NKTO-700, i.e., the larger S_{BET} of the sample is, the higher activity of the sample is, which is just contrary to the result from UV-vis spectra (Fig. 10a), highlighting the S_{BET} is a more primary factor in determining the photocatalytic activity of NKTO nanobelts than optical adsorption. This is just why P25 with high S_{BET} of 45.71 m^2/g (Fig. S4, close to the previous report[48]) exhibit the best activity, considering that high S_{BET} means strong adsorption ability of a photocatalyst and then enhance its photocatalytic efficiency. The absorption of MO in dark for 1h is 10.46%, 5.34%, 4.20% and 3.81% for P25, NKTO-660, NKTO-680 and NKTO-700, respectively, which accords with their S_{BET} .

Combined with the fact that NKTO-800 preform higher activity than NKTO-900, it could be concluded that the lower synthetic temperature resulted in a better performance in photocatalysis. Besides, the comparative studies between NKTO-900 and KTO-900 as well as NTO-900 revealed that substitutional Na-modifying greatly contributed to an increase

in the photocatalytic activity, which could be ascribed to the efficient separation of photogenerated electron-hole pairs, smaller Eg as well as the enhencement of optical absorption.

3.7 Possible mechanism of improved photocatalytic activity

Based on the results above, we can conclude that photocatalytic activity of the samples is governed by some crucial factors, such as phase composition, S_{BET}, adsorption ability, and separation efficiency of photogenerated electrons and holes. Except the low temperature synthesis resulting in high S_{BET}, the substitutional Na-modifying changes the phase composition and band structure, which is deemed to play a vital role in improving the photocatalytic activity.[49-51]

From this angle, a possible mechanism for improved photocatalytic activity of NKTO nanobelts was tentatively proposed and illustrated in Fig. 13. The conduction band and valence band potentials (named as E_{CB} and E_{VB}) of the semiconductors could be calculated by the following equation:

$$E_{VB} = \chi - E_0 + 1/2E_g$$
$$E_{CB} = \chi - E_0 - 1/2E_g \quad (5)$$

in which χ is the absolute electronegativity of the semiconductor, determined by the geometric mean of the absolute electronegativity of constituent atoms, which is defined as the arithmetic mean of the atomic electron affinity and the first ionization energy; E_0 is the energy of free electrons on the hydrogen scale (~ 4.5 eV).[52] The calculated E_{CB} and E_{VB} for $K_2Ti_6O_{13}$, $Na_2Ti_6O_{13}$, and $Na_{0.88}K_{1.12}Ti_6O_{13}$ were shown in Fig. 13, respectively.

The E_{CB} of NKTO is negative to the redox potential of $O_2/^{\cdot}O_2^-$ (-0.13 eV *vs.* NHE),[53] implying that the photogenerated electrons can react with O_2 dissolved in the solution to produce $^{\cdot}O_2^-$ radicals that are the important active species involved in photocatalysis. Moreover, the E_{VB} of NKTO is more positive than the standard redox potential of $OH^-/^{\cdot}OH$ (1.99 eV *vs.* NHE),[54] suggesting that the holes on the surface of NKTO can oxidize OH^- into active $^{\cdot}OH$ radicals. It is noted

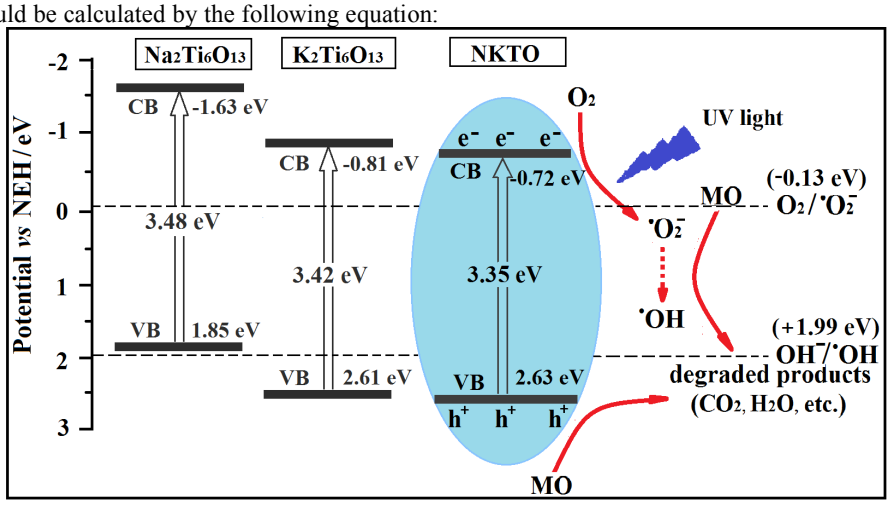

Fig. 13 Schematic diagram for the band structure of $K_2Ti_6O_{13}$ and $Na_2Ti_6O_{13}$ and the possible photocatalytic mechanism of NKTO nanobelts.

that the E_{CB}/E_{VB} of NKTO move downwards about 0.90 eV/0.78 eV and 0.08 eV/0.02 eV with respect to those of $Na_2Ti_6O_{13}$ and $K_2Ti_6O_{13}$, respectively, which may contribute to produce a high amount of active radicals for photocatalytic reactions from the harvested photons by the following reaction:[50]

$$NKTO + h\nu \rightarrow e^- + h^+$$
$$O_2 + e^- \rightarrow {}^{\cdot}O_2^-$$
$$^{\cdot}O_2^- + 2H^+ + e^- \rightarrow H_2O_2$$
$$H_2O_2 + H^+ + e^- \rightarrow {}^{\cdot}OH + H_2O$$
$$H_2O_2 + {}^{\cdot}O_2^- \rightarrow {}^{\cdot}OH + OH^- + O_2$$
$$H_2O_2 + h\nu \rightarrow 2{}^{\cdot}OH$$
$$^{\cdot}O_2^-, {}^{\cdot}OH, h^+ + MO \rightarrow \text{degraded products } (CO_2, H_2O, \text{etc})$$

Apparently, $^{\cdot}O_2^-$, $^{\cdot}OH$ and H_2O_2 act as the efficient e^- traps, suppressing the recombination of the photogenerated electrons and holes to improve the photocatalytic activity. Besides, the improved photocatalytic activity could be also attributed to the dipole moment due to the distortion of TiO_6 octahedra induced by the replacement of K^+ by Na^+ ions promoting photogenerated charges separation.[55]

4. Conclusions

In summary, high-quality NKTO nanobelts with enhanced ultraviolet photocatalytic activity have been synthesized via a facile one-step method from NaCl-KCl melts at a relatively

low temperature below 700 □. The substitutional Na ions were incorporated into $K_2Ti_6O_{13}$ without destroying its tunnel-like structure and oriented growth along [010] direction. Based on these results, the formation mechanism of NKTO nanobelts was proposed and rutile was found to be the optimum titanium precursor. The substitutional Na modifying and low-temperature synthesis not only red-shifted the edge, enhanced the absorption intensity and enlarged surface area but also effeciently suppressed the recombination of photogenerated electron-hole pairs, whcih was studied to improve the photocatalytic activity of NKTO nanobelts. And, the possible photocatalytic mechanism was also discussed. Therefore, the low temperature (<700 □) one-step synthesis of NKTO nanobelts from NaCl-KCl melts is not only facile and cost-effective but also greatly beneficial to improve the photocatalytic properties and this study will be inspiring for efficiently preparing and modifying other functional materials.

References

[1] D.M. Yu, J.S. Wu, L.M. Zhou, D.R. Xie and S.Z. Wu, Compos. Sci. Technol., 2000, 60, 499–508.
[2] X.K. Zhang, S.L. Tang , L. Zhai, J.Y. Yu, Y.G. Shi and Y.W. Du, Mater. Lett., 2009, 63, 887–889.
[3] S.O. Kang, H.S. Jang, K.I. Kim, K.B. Kim and M.J. Jung, Mater. Lett., 2007, 61, 473–477.
[4] Y.C. Kim, M.H. Cho, S.J. Kim and H. Jang, Wear, 2008, 264, 204–210.
[5] J.Z. Lü and X.H. Lu, J. Appl. Polym. Sci., 2001, 82, 368-374.
[6] S.Q. Wu, Z.S. Wei and S.C. Tjong, Compos. Sci. Technol., 2000, 60, 2873–2880.
[7] H.X. Zhang, X.D. He and F. He, J. Alloys Compd., 2009, 472, 194.
[8] D.V. Bavykin and F.C. Walsh, J. Phys. Chem. C, 2007, 111, 14644.
[9] T.W. Kim, I.Y. Kim, J.H. Im, H.-W. Ha and S.-J. Hwang, J. Photoch. photobio. A: Chem., 2009, 205, 173–178.
[10] J. Park, J. Alloys Compd., 2010, 492, 57–60.
[11] X.K. Zhang, J.J. Yuan, H.J. Yu, X.R. Zhu, Z. Yin and H. Shen, J. Alloys Compd., 2015, 631, 171–177.
[12] L. Zhen, C. Y. Xu, W.S. Wang, C.S. Lao and Q. Kuang, Appl. Surf. Sci., 2009, 255, 4149.
[13] V. Štengl, S. Bakardjieva, J. Šubrt, E. Večerníková, L. Szatmary, M. Klementová and V. Ba lek, Appl. Catal. B: Environ., 2006, 63, 20-30.
[14] M. A. Siddiqui, V. S. Chandel and A. Azam, Appl. Surf. Sci., 2012, 258, 7357.
[15] Y. Inoue, T. Kubokawa and K. Sato, J. Chem. Soc., Chem. Commun., 1990, 1298.
[16] S. Ogura, M. Kohno, K.Sato and Y. Inoue, Phys. Chem. Chem. Phys., 1999, 1, 179-183.
[17] S. Ogura, M. Kohno, K. Sato and Y. Inoue, Appl. Surf. Sci., 1997, 121/122, 521- 524.
[18] J. Ramírez-Salgado, E. Djurado and P. Fabry, J. Eur. Ceram. Soc., 2004, 24, 2477.
[19] C.Y. Liu, H.B. Yin, Y.M. Liu, M. Ren, A.L. Wang, C. Ge, H.P. Yao, H. Feng, J. Chen and T.S. Jiang. Mater. Res. Bull., 2009, 44, 1173-1178.
[20] N. Bao, L. Shen, X. Feng and X. Lu, J. Am. Ceram. Soc., 2004, 87, 326.
[21] Q. Wang, Z. Guo and J.S. Chung, Mater. Res. Bull., 2009, 44, 1973–1977.
[22] Y. Hakuta, H. Hayashi and K. Arai. J. Mater. Sci., 2004, 39, 4977-4980.
[23] T. Zhang, Q. Chen and L. M. Peng. Adv. Funct. Mater., 2008, 18, 3018-3025.
[24] B.L. Wang, Q. Chen, R.H. Wang and L.M. Peng, Chem. Phys. Lett., 2003, 376, 726.

Acknowledgements

This work was supported by National Natural Science Foundation of China (No.51274102).

[25] X.D. Meng, D.Z. Wang, J.H. Liu, B.X. Lin and Z.X. Fu, Solid State Commun., 2006, 137, 146.
[26] L. M. Torres-Martínez, I. Juárez-Ramírez, K.D. Ángel-Sánchez, L. Garza-Tovar, A. Cruz-López and G. Del Ángel, J. Sol-Gel. Sci. Technol., 2008, 47, 158-164.
[27] K. Teshima, K. Yubuta, T. Shimodaira, T. Suzuki,M. Endo, T. Shishido and S. Oishi, Cryst. Growth Des., 2008, 8, 465-469.
[28] C.Y. Xu, Q. Zhang, H. Zhang, L. Zhen, J. Tang and L.C. Qin, J. Am. Chem. Soc., 2005, 127, 11584-11585.
[29] L.Q. Xu and L. Cheng, Mater. Charact., 2010, 61, 245-248.
[30] S. Suzuki, K. Teshima, M. Kiyohara, H. Kamikawa, K. Yubuta, T. Shishido and S. Oishi, CrystEngComm, 2012, 14, 4176-4180.
[31] Y.B. Mao, T. Park, F. Zhang, H.J. Zhou and S. Wong, Small, 2007, 3, 1122.
[32] Q. Wang, Q.J. Guo, H. Wang and B. Li, Mater Letter, 2015, 155, 38.
[33] C.Y. Xu, Y.Z. Liu, L. Zhen and Z.L. Wang, J. Phys. Chem., C, 2008, 112, 7547-7551.
[34] C.Y. Xu, J. Wu, P. Zhang, S.P. Hu, J.X. Cui, Z.Q. Wang, Y.D. Huang and L. Zhen, CrystEngComm, 2013, 15, 3448-3453.
[35] E.V. Tretyachenko, A.V. Gorokhovsky, G.Y. Yurkov, F.S. Fedorov, M.A. Vikulova, D.S. Kovaleva and E.E. Orozaliev, Particuology, 2014, 17, 22-28.
[36] F. Amano, T. Yasumoto, T. Shibayama, S. Uchida and B. Ohtani, Appl. Catal. B: Environ., 2009, 89, 583.
[37] S. Tawkaew, M. Chareonpanich and S. Supothina, Mater. Chem. Phys., 2008, 111, 232.
[38] T. Zaremba. Mater. Sci-Poland, 2012, 30, 185.
[39] B.R. Li, W. Shang, Z.L. Hu and N.Q. Zhang, Ceram. Int., 2014, 40, 78.
[40] P.M. Rørvik, T. Lyngdal and R. Sæterli, Inorg. Chem., 2008, 47, 3173.
[41] H.B. He,W.J. Yao,C.S. Wang, X. Feng and X.H. Lu, Ind. Eng. Chem. Res., 2013, 52, 15037.
[42] K.S.W. Sing, D.H. Everett, R.A.W. Haul, L. Moscou, R.A.Pierotti, J. Rouquerol and T. Siemieniewska, Pure Appl. Chem., 1985, 57, 603–619.
[43] J. Zhang, S.Z. Hu and Y.J. Wang, RSC Adv., 2014, 4, 62914.
[44] F. Chang, Y.C. Xie, J. Zhang, J. Chen, C.L. Li, J. Wang, J.R. Luo, B.Q. Deng and X.F. Hu, RSC Adv., 2014, 4, 28519-28528.
[45] S.D. Delekar, H.M. Yadav, S.N. Achary, S.S. Meena and S.H. Pawar, Appl. Surf. Sci., 2012, 263, 539.
[46] B. Yue, Q.Y. Li, H. Iwai, T. Kako and J.H. Ye, Sci. Technol. Adv. Mater., 2011, 12, 034401.
[47] G.H. Du, Q. Chen, P.D. Han, Y. Yuan and L.-M. Peng, Phys. Rev., B, 2003, 67, 035323.
[48] K. Sridharan, E. Jang and T. J. Park, Appl. Catal. B: Environ., 2013, 142-143, 718-728.

[49] H. Kato, H. Kobayashi, and A. Kudo, J. Phys. Chem. B, 2002,106, 12443.
[50] F.Z. Ren, J.H. Zhang and Y.X. Wang, RSC Adv., 2015, 5, 29058.
[51] Z. Zou, J. Ye and H. Arakawa, Chem. Phys. Lett., 2000, 332, 271-277.
[52] X.J. Guan and L.J. Guo, ACS Catal., 2014, 9, 3025.
[53] W.Y. Teoh, J.A. Scott and R. Amal, J. Phys. Chem. Lett., 2012, 3, 629-639 .
[54] L. Kong, Z. Jiang, T. Xiao, L. Lu, M.O. Jones and P.P. Edwards, Chem. Commun., 2011, 47, 5512-5514.
[55] A. Kudo, H. Kato and S. Nakagawa, J. Phys. Chem. B, 2000, 104, 571-575.

Graphical Abstract

High-quality substitutional Na-modified $K_2Ti_6O_{13}$ nanobelts with improved photocatalytic activity were synthesized efficiently from NaCl-KCl melts below 700□.